RsaM: a transcriptional regulator of *Burkholderia* spp. with novel fold

Karolina Michalska[1,2], Gekleng Chhor[1], Shonda Clancy[1], Robert Jedrzejczak[1], Gyorgy Babnigg[1], Stephen C. Winans[3] and Andrzej Joachimiak[1,2,4]

1 Midwest Center for Structural Genomics, Argonne National Laboratory, IL, USA
2 Structural Biology Center, Biosciences Division, Argonne National Laboratory, IL, USA
3 Department of Microbiology, Cornell University, Ithaca, NY, USA
4 Department of Biochemistry and Molecular Biology, University of Chicago, IL,USA

Burkholderia cepacia complex is a set of closely related bacterial species that are notorious pathogens of cystic fibrosis patients, responsible for life-threatening lung infections. Expression of several virulence factors of *Burkholderia cepacia* complex is controlled by a mechanism known as quorum sensing (QS). QS is a means of bacterial communication used to coordinate gene expression in a cell-density-dependent manner. The system involves the production of diffusible signaling molecules (*N*-acyl-L-homoserine lactones, AHLs), that bind to cognate transcriptional regulators and influence their ability to regulate gene expression. One such system that is highly conserved in *Burkholderia cepacia* complex consists of CepI and CepR. CepI is AHL synthase, whereas CepR is an AHL-dependent transcription factor. In most members of the *Burkholderia cepacia* complex group, the *cepI* and *cepR* genes are divergently transcribed and separated by additional genes. One of them, *bcam1869*, encodes the *Bc*RsaM protein, which was recently postulated to modulate the abundance or activity of CepI or CepR. Here, we show the crystal structure of *Bc*RsaM from *B. cenocepacia* J2315. It is a single-domain protein with unique topology and presents a novel fold. The protein is a dimer in the crystal and in solution. This regulator has no known DNA-binding motifs and direct binding of *Bc*RsaM to the *cepI* promoter could not be detected in *in vitro* assays. Therefore, we propose that the modulatory action of RsaM might result from interactions with other components of the QS machinery rather than from direct association with the DNA promoter.

Introduction

The *Burkholderia* species are betaproteobacteria that inhabit various ecosystems (reviewed in [1]), where they play a wide variety of ecological roles. For example, some species colonize the rhizosphere and engage in symbiosis that promotes plant growth. Some form nodules on the roots of legumes and are capable of fixing atmospheric nitrogen. They also occur naturally in water and soil, where they could potentially be exploited in bioremediation due to their ability to degrade a number of toxic compounds, including oil-derived pollutants and xenobiotics (reviewed in [2]). However, besides their positive relationships with other organisms and the environment, *Burkholderia* are also known as precarious human and plant pathogens, which raises safety concerns for their biotechnological applications.

Burkholderia cepacia complex is a group of at least 18 species [3–6]. Some members are recognized as causative agents of pneumonia in immunocompromised patients with a pre-existing lung disease, such as cystic fibrosis or chronic granulomatous disease. The most commonly identified pathogenic species in affected individuals are *B. cenocepacia* and *B. multivorans* [7]. In cystic fibrosis patients, *Burkholderia* is the second major pathogen responsible for chronic lung infection, with *Pseudomonas aeruginosa* holding the dishonorable first place. In extreme cases, *Burkholderia*-associated inflammation, induced by antibiotic resistant species, leads to the so-called 'cepacia syndrome' – a condition manifesting in high fever, leukocytosis and progressive respiratory failure with poor prognosis of survival [8]. The molecular mechanisms of *B. cenocepacia* pathogenicity remain poorly understood. A detailed research of the *Burkholderia* species, and the *B. cenocepacia* epidemic lineage ET–12, in particular, enabled the identification of a number of virulence factors critical for bacterial invasion [9].

Expression of several virulence-related genes in *B. cenocepacia* is controlled by quorum sensing (QS) systems (reviewed in [10]). QS is a method of social communication that enables bacteria to coordinate the behavior of their community in a cell-density-dependent manner. QS systems rely on the synthesis of small signaling molecules (autoinducers), their passive diffusion or active transport across the cell envelope [11–13] and their receptor-mediated detection by members of the same species. In proteobacteria, these signals are most often *N*-acyl-L-homoserine lactones (AHL). These compounds reprogram the gene transcription pattern to induce physiological processes that are beneficial for a larger bacterial population but could be nonproduc-

tive for individual cells. A typical QS system requires an AHL synthase that resembles LuxI of *Vibrio fischeri* and an AHL-dependent transcription factor that resembles the *V. fischeri* LuxR protein. As the bacterial population grows, AHL accumulates intra- and extracellularly until it reaches a critical level. At sufficiently high concentrations, AHL binds to and activates the LuxR-type regulator, which subsequently affects the expression of QS-controlled target genes, including QS genes themselves. A small number of LuxR-type proteins are active only as apoproteins and are functionally inactive when binding their cognate AHL [14]. Most LuxR-type proteins are transcription activators, but a few can function as transcriptional repressors.

All known species of *Burkholderia* encode proteins orthologous to the *cepI* and *cepR* genes of *B. cenocepacia* [15,16]. These systems consist of a CepR transcription regulator and CepI autoinducer synthase that generates primarily *N*-octanoyl-L-homoserine lactone (OHL). CepI can also synthesize *N*-hexanoyl-L-homoserine lactone when overexpressed in *Escherichia coli* [17]. Besides CepIR, virulent *B. cenocepacia* strains encode the CciIR system that is found on the cenocepacia island (cci) [18]. CciI produces *N*-hexanoyl-L-homoserine lactone and small amounts of OHL. For the most part, CepR operates as an activator, whereas CciR acts as a repressor of the same pool of genes. In addition, some isolates of *B. cenocepacia* encode an additional LuxR-type protein called CepR2. CepR2 lacks a cognate AHL synthase and is therefore designated an orphan receptor. In one study, CepR2 was reported to function independently of AHLs [19], although a second study demonstrated that CepR2 functions only as an apoprotein and that its action is inhibited by OHL [20]. Apo-CepR2 represses several promoters located near the *cepR2* gene [19,20]. All *B. cenocepacia* QS mechanisms have complex regulatory connections and work together in an orchestrated manner. These relationships have been recently thoroughly reviewed by Subramoni & Sokol [10].

Recently, it became recognized that the QS response might be further modulated by additional factors present on QS loci. *luxIR* modules show a number of different chromosomal arrangements within the QS loci. In the simplest scenarios, the two genes are located next to each other and are transcribed either divergently, convergently or in the same direction (e.g. *cciIR*) [21]. In more intricate cases, the *lux* genes are separated by one or more additional genes, multiplying the number of possible genetic architectures. QS loci may also contain other genes present outside the *luxIR*-encoding region. The two latter situations may be illustrated by the *B. cenocepacia cepIR* locus (Fig. 1A),

which contains *bcam1869* and *bcam1871* QS-related genes. *bcam1869* is localized in between the divergent *cepR* and *cepI* genes and is transcribed in the same direction as *cepI*. *bcam1871* is positioned downstream of *cepI* and is cotranscribed with *cepI*. Both these genes have recently been shown to be activated by CepR–OHL complexes [22–25].

The *bcam1869* product, here designated as *Bc*RsaM, is the focus of this study, which was undertaken because of reports suggesting that its homologs play modulatory roles in QS [22]. A homolog of *Bc*RsaM, the RsaM protein from *Pseudomonas fuscovaginae*, was identified as part of the QS system of that organism [22]. *P. fuscovaginae* contains two QS systems, PfvIR
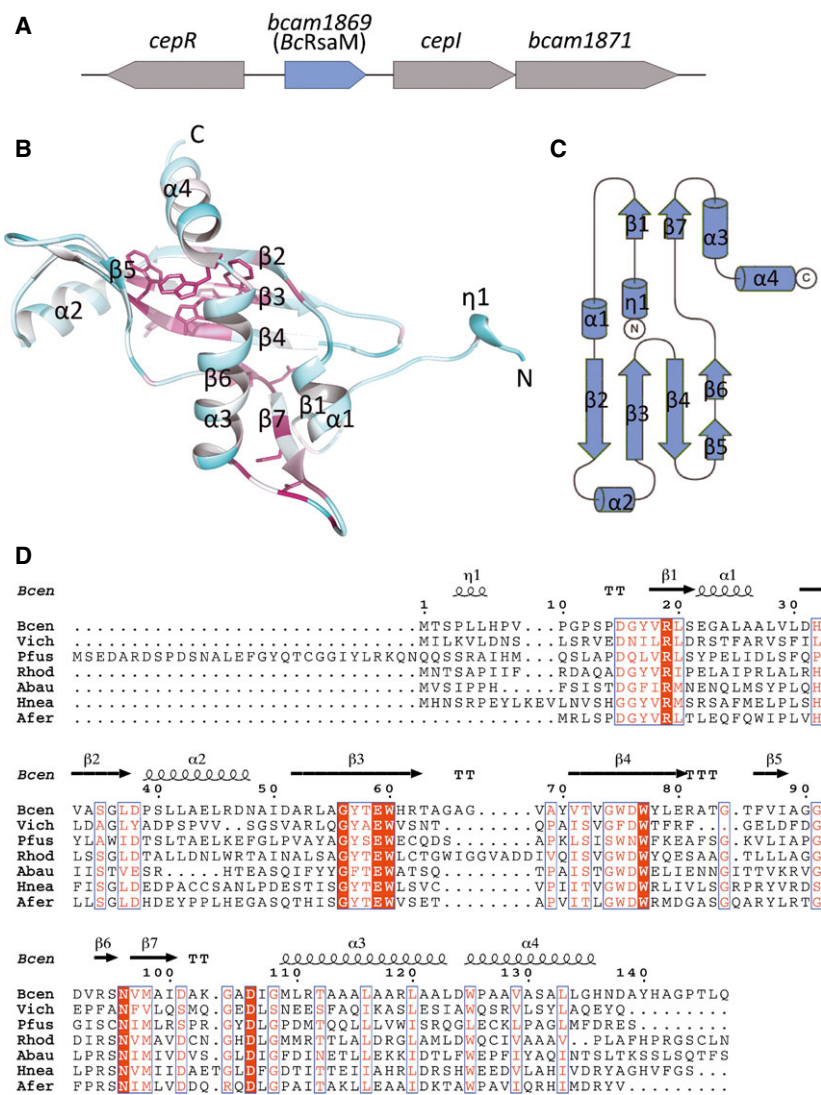

Fig. 1. The *bcam1869* gene of *B. cenocepacia* and its product, *Bc*RsaM protein. (A) Genetic organization of the *B. cenocepacia bcam1869* locus. The *bcam1869*, *cepI* and *bcam1871* genes are transcriptionally induced by CepR–OHL complexes [25]. (B) Overall fold of the *B. cenocepacia Bc*RsaM monomer colored according to sequence conservation, with the most conserved residues shown in maroon (also in a stick representation) and the most variable shown in cyan. (C) Topology diagram of *Bc*RsaM. (D) Multiple sequence alignment of *B. cenocepacia Bc*RsaM with a subset of homologs: Bcen, *B. cenocepacia J2315* (gi|206563717); Vich, *V. ichthyoenteri* (gi|493766304); Pfus, *P. fuscovaginae* (gi|290454886); Rhod, *Rhodanobacter* sp. *115* (gi|495487176); Abau, *A. baumannii* (gi|491275299); Hnea, *H. neapolitanus c2* (gi|261855566), Afer, *A. ferrooxidans ATCC 53993* (gi|198283773). The alignment was generated using the Muscle algorithm [59] and displayed using ESPRIPT [60]. Strictly conserved residues are shown in white on a red background, moderately conserved ones are in red. The secondary structure elements for *Bc*RsaM are shown above the alignment with α corresponding to α helices, β to β strands and η to helix 3₁₀. T indicates turns.

and PfsIR, with the *rsaM* gene localized between *pfsR* and *pfsI*. Strikingly, the majority of *cepR* and *cepI* genes found in *Burkholderia* spp. are separated by a gene that resembles *rsaM* [26]. Generally, genome-wide analyses indicate that the presence of *rsaM*-like genes is limited to β- and γ-proteobacteria with AHL-QS systems [27]. This group includes *Burkholderia* spp., *Acinetobacter baumannii*, *Acidithiobacillus ferrooxidans*, *Halothiobacillus neapolitanus* and, as mentioned earlier, *P. fuscovaginae* [27]. In all genomes, the *rsaM* genes are found directly adjacent to the *luxI* homolog and are oriented in the same direction. Most commonly, it also neighbors the *luxR*-family gene, but occasionally these two genes are separated by additional open reading frames. There are also examples of *rsaM* homologs that lack a nearby *luxR* gene (in *B. cepacia* AMMD and *B. ambifaria* MC40-6 strains) [26].

The RsaM protein from *P. fuscovaginae* and its homolog from the *B. cenocepacia* H111 strain have been shown to downregulate AHL production [22,28]. This phenomenon has been attributed to repression of the *luxI*-like gene transcription, although post-transcriptional mechanisms have also been considered [28]. Remarkably, in the *P. fuscovaginae* study, RsaM not only influenced expression of its cognate AHL synthase, PfsI, but also inhibited PfvR-dependent *pfvI* transcription, despite the fact that the PfvIR system contains its own repressor, RsaL. A series of experiments with the *B. cenocepacia* H111 QS system also demonstrated that its *Bc*RsaM protein influences expression or activity of the CepIR system as well as the CepR2 regulator [28]. Consequently, it affects transcription of Cep-regulated downstream genes. Therefore, RsaM appears to be a major regulatory protein that fine-tunes the QS apparatus in β- and γ-proteobacteria.

Because *Bc*RsaM shares no sequence similarity with biochemically or structurally characterized proteins, the molecular basis of its modulatory action remains to be discovered. We have undertaken crystallographic studies and biochemical characterization of *Bc*RsaM of *B. cenocepacia* strain J2315, hoping that structural information will provide some insights into the physiological function of *Bc*RsaM in QS systems. Here, we present the *Bc*RsaM crystal structure determined at 2.3 Å resolution and biochemical characterization of the protein.

Results and discussion

Overall fold

*Bc*RsaM is a one-domain protein (147 amino acid residues) with a melting temperature of 43.5 ± 0.5 °C. The core of the molecule consists of a five-stranded antiparallel β sheet (strands ↑-β2, ↓-β3, ↑-β4, ↓-β5 and ↓-β6) that wraps around two α helices (α3 and α4, Fig. 1B). The two pairs of chains, namely β3–β4 and β4–β5, are β hairpins. The β5 and β6 elements are also consecutive elements of the polypeptide molecule, but instead of creating a turn, they adopt an extended conformation, with both β strands interacting with β4. Therefore, for topological purposes, β5 and β6 could be considered as one β chain with an internal loop. The fold is completed by additional elements decorating the central module. These include a parallel β sheet (strands β1 and β7) as well as helices α1 and α2. The N-terminus of the molecule protrudes from the otherwise globular molecule and adopts the conformation of a 3_{10} helix, designated as η1.

Similarity to other proteins

A search for structural homologs using the Dali server [29] does not reveal any significant hits; all 129 nonredundant hits have *Z*-scores < 4.0. Nevertheless, as the central structural motif (a β sheet gripped around an α helix) is not without precedent, some curious matches were identified. For example, the retrieved entries of comparable size to *Bc*RsaM include papain (*Z*-score 2.6, r.m.s.d. 2.8 Å, 55 aligned residues, PDB 3IMA), cystatins (cystatin 2: *Z*-score 2.4, r.m.s.d. 2.7 Å, 57 aligned residues, PDB 3L0R) and Der f 7 allergen (*Z*-score 3.2, r.m.s.d. 4.2 Å, 90 aligned residues, PDB 3UV1). Possibly the closest structural analogy can be observed with protein p22 from *Trypanosoma brucei* (*Z*-score 3.6, r.m.s.d. 3.5 Å, 79 aligned residues, PDB 3JV1). Another interesting distant relative is a SpoVG protein (*Z*-score 3.5, rmsd 3.2 Å, 69 aligned residues, PDB 2I9X). As shown in Fig. 2, the overall architecture of the protein core clearly resembles those mentioned above, which enables us to classify it as an (α/β)-roll, but its topology is very different. Therefore, we conclude that *Bc*RsaM has a novel protein fold. Moreover, it does not appear to possess any known DNA-binding motifs. Interestingly, the family of SpoVG has been shown recently to interact with DNA specifically [30]. A detailed comparison between SpoVG and *Bc*RsaM reveals that our protein does not contain the key β hairpin. That element in SpoVG bears conserved, positively charged residues crucial for DNA binding. In addition, the SpoVG dimer does not resemble any of the assemblies observed for *Bc*RsaM (see below).

Oligomeric state

Size-exclusion chromatography and dynamic light scattering experiments indicated that the *Bc*RsaM protein
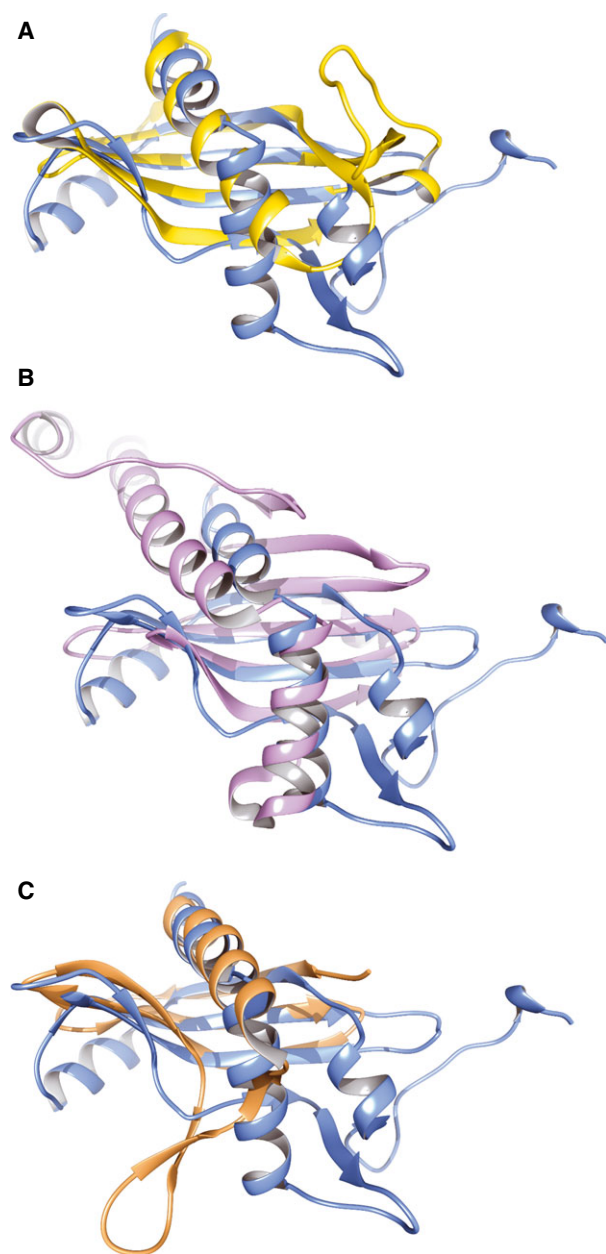
A

B

C

Fig. 2. Superposition of the *Bc*RsaM monomer with human cystatin C (A, PDB entry 3NX0), with *T. brucei* p22 (B, PDB entry 3JV1) and with SpoVG (C, PDB entry 2I9X).

is a dimer in solution (26.1 and 34.0 kDa for the two methods with the same protein concentration, respectively, Fig. 3). With a twofold noncrystallographic and high crystal symmetry, the protein molecules contact with one another through several dimer-like interfaces. As calculated by the PISA server [31], four of them [designated as D1(A), D2(A), D2(B), D3(AB)] involve a buried area > 1000 Å^2 (per dimer, Fig. 4) and are considered as potential quaternary structures. The D1

(A) assembly (Fig. 4A) can be described as a face-to-face dimer. It is created by molecule A and its crystallographic mate A′ (*x–y*, -*y*, -*z*) with hydrophobic helices α3 being the main interacting elements. Four hydrogen bonds link additional protein fragments as Glu22 (α1) of each subunit binds to Tyr78 (β4) and Gly90 (β5) of the opposite subunit. The dimer generates 1490 Å^2 of buried area, which is ~ 10% of the total surface area. However, the predicted ΔG^{diss} is low (1.3 kcal·mol^{-1}) and the two molecules do not contact with each other through the entire interface area, i.e. two channels are present between the protein chains. Moreover, monomers B do not form an identical arrangement. Although an analogous pattern could be identified, with two B molecules having similar orientations as within the D1(A) assembly, translational components keep the monomers separated (only 53 Å^2 of interface area per monomer). These observations suggest that dimer D1(A) is most likely a crystallographic artifact.

Dimer D2(A) (Fig. 4B) consists of molecule A and its crystallographic copy A′ generated through -*y*, -*x*, -*z*-⅙ operation. The A–A′ assembly generates 1840 Å^2 (13% of the total surface area) of buried area. An equivalent dimer D2(B) created by monomers B provides a comparable buried area (1820 Å^2) suggesting that the two D2 oligomers represent the same protein state. Nevertheless, both D2 variants have low ΔG^{diss} (1.7 kcal·mol^{-1} for A). In fact, the predicted ΔG^{diss} for the B-molecule-based dimer is even lower than for the A–A′ dimer. D2 associations are created by back-to-back interaction of the β sheets. It appears to be mostly hydrophobic as no direct protein–protein hydrogen bonds could be found.

The above dimers have rather globular shapes but a more elongated particle, D3(AB) (Fig. 4C), could also be identified. It includes two polypeptide chains present in the asymmetric unit. However, the buried area of this arrangement is low (1040 Å^2) and its predicted ΔG^{diss} has the lowest value from all possible assemblies (−0.9 kcal·mol^{-1}), which indicates an unstable arrangement. The molecules contact each other through their N-terminal, proline-rich regions (L^{6}HPVPGPS^{13}). Although the interacting fragments do not form typical β strands that could be recognized by secondary structure analyzing programs, such as DSSP [32], they do generate an intermolecular β-sheet-like association with four main-chain–main-chain hydrogen bonds and two additional side-chain–main-chain interactions (Fig. 4C).

Curiously, some of the RsaM family members are shorter and do not contain the η1–β1 stretch. However, there are also homologs with extra elements on the
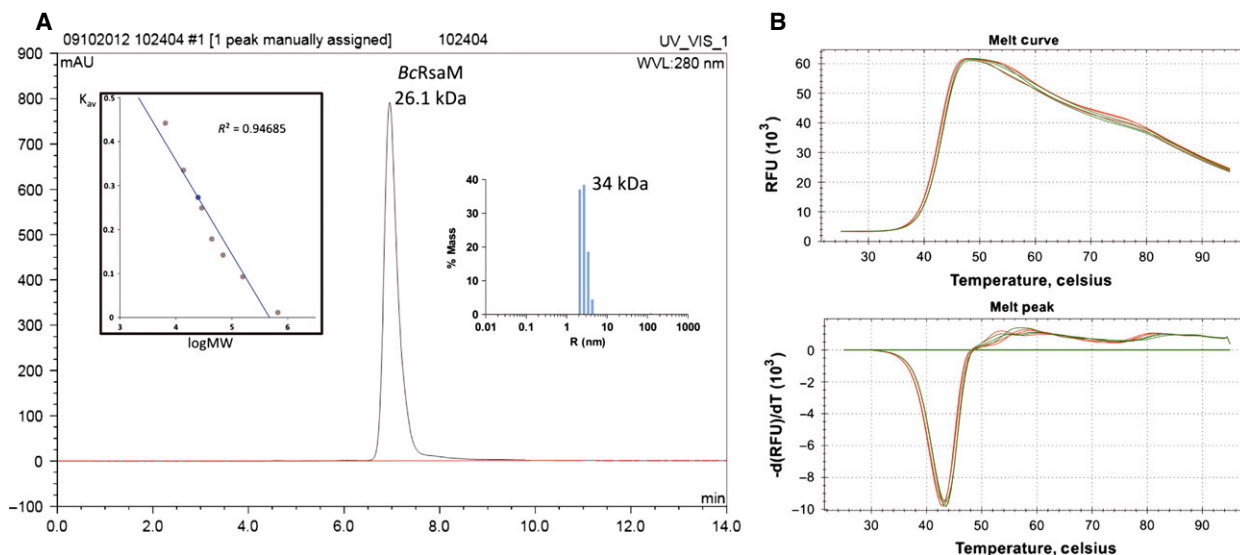
Fig. 3. *Bc*RsaM characterization. (A) Molecular weight determination of *Bc*RsaM using size-exclusion chromatography and dynamic light scattering. The absorbance at 280 nm is plotted in absorbance units (AU) versus retention time in min. (Left) Plot of K_{av} coefficient versus logarithm of molecular weight [red circles correspond to standard proteins: 1, aprotinin (6.5 kDa); 2, ribonuclease A (13.7 kDa); 3, carbonic anhydrase (29 kDa); 4 ovalbumin (44 kDa); 5, conalbumin (75 kDa); 6, aldolase (158 kDa); 7, thyroglobulin (669 kDa); blue circle corresponds to *Bc*RsaM (26.1 kDa)]. A clear peak is observed for the *Bc*RsaM dimer, no other species were detected. (Right) dynamic light scattering results representing particle size distribution for *Bc*RsaM. (B) Differential scanning fluorimetry data for *Bc*RsaM alone (green) and in the presence of OHL (red). (Upper) Melting curve. (Lower) First derivative.

N-terminus (~ 120 amino acids longer than *Bc*RsaM). The variability of the N-terminus and high sequence conservation of the solvent-exposed face of the β sheet (see below) suggest that dimers D2 [D2(A)/D2(B)], with two molecules interacting back-to-back, may represent the biologically relevant oligomeric state of *Bc*RsaM. That is also consistent with the size-exclusion chromatography data: the apparent molecular weight of the protein is less (26.1 kDa) than the predicted value from the *Bc*RsaM amino acid sequence (31.0 kDa), which indicates a compact, globular shape. The D2 dimer has the largest interface with several conserved residues (Glu59, Asp76, Arg94 and Asn96 patch, see below), it can easily accommodate gene extensions and insertions present in the family, shows good surface electrostatic complementarity and there are a number of hydrophobic residues that are buried on the interface. We believe that *Bc*RsaM is not capable of forming a dimer observed in DNA-binding SpoVG.

Sequence conservation

Mapping of the PSI-BLAST-based sequence conservation on the protein structure reveals three conserved regions (Figs 1D and 4). The most striking is the core of the molecule occupied by a quartet of strictly preserved tryptophan residues (Trp60, Trp75, Trp77 and Trp125). This hydrophobic core cluster is clearly a unique feature of the RsaM fold. An additional patch of conserved residues is found facing the protein interior, including residues Leu30, Leu116, Thr58 and Ser95. On the protein surface, two regions seem to be maintained across the protein family. One is created by the solvent-facing part of the β sheet and includes Asp76, a salt bridge between Arg94 and Glu59, and the neighboring Asn96 (part of the D2 dimer interface). The second solvent-exposed conserved fragment is created by the β1–β7 sheet and the loop following the β7 strand, with residues Met98, Gly104, Asp106 and Gly108 being the least variable. The conformation of this protein segment is maintained not only through the main-chain-main-chain hydrogen bonds within the β sheet, but also additional interactions, including bifurcated salt bridging of Arg19 (with Asp15 and Asp106) and a side-chain–main-chain hydrogen bond between Asp101 and Gly104 within a β turn (seen only in chain A; an equivalent fragment of chain B has not been modeled due to poor electron density).

Functional implications

To the best of our knowledge, neither RsaM of *B. cenocepacia* nor any homologous proteins have been subjected to thorough biochemical analysis. However,
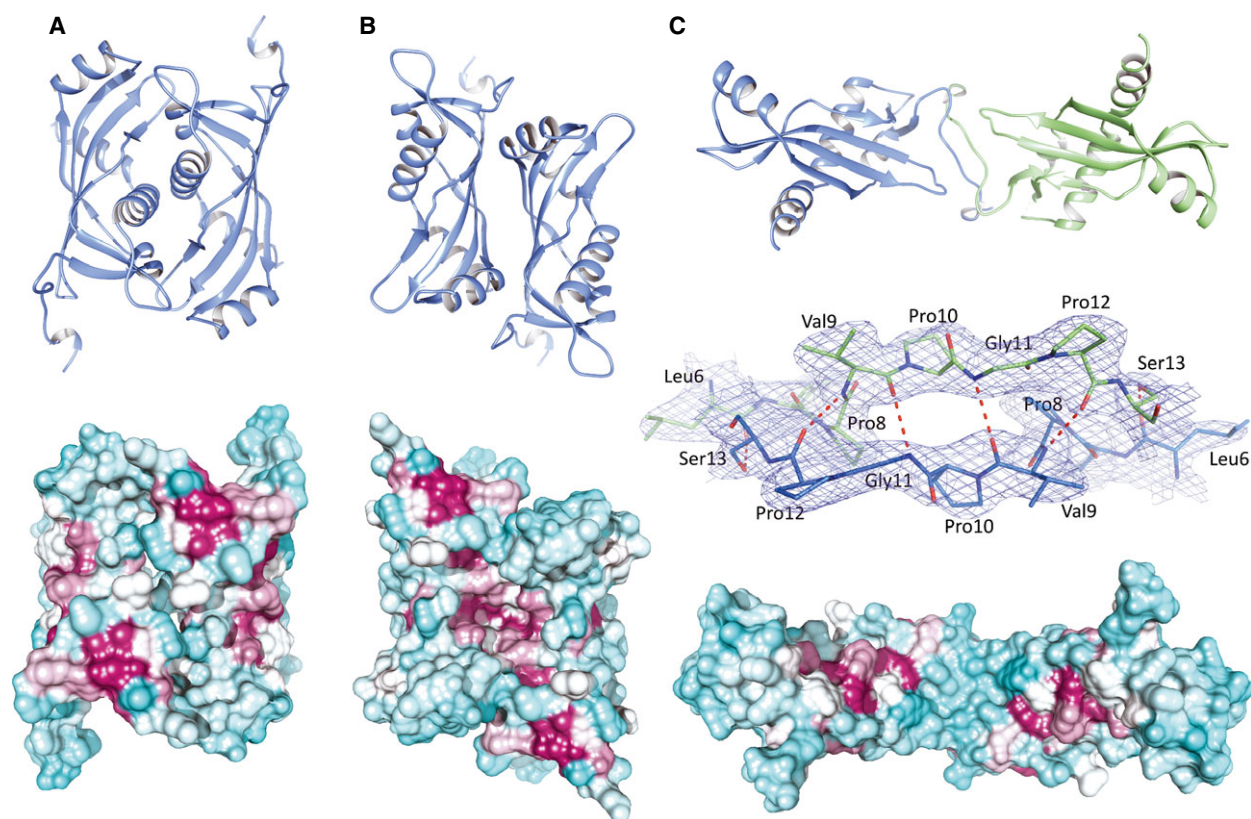
Fig. 4. Potential dimers of *Bc*RsaM. In the cartoon models (upper), chains are colored according to crystallographic monomers involved in the dimer, with molecule A (or its crystallographic copy) shown in blue and molecule B shown in green. The molecular surfaces (lower) are colored according to sequence conservation with maroon indicating conserved residues and cyan showing nonconserved ones. Sequence conservation calculation was done in CHIMERA [61] based on 120 sequences identified in three iterations of PSI-BLAST at NCBI and aligned in the MUSCLE program [59]. The molecules are oriented to present their more conserved side. For (C), the middle picture presents the dimer interface shown in 2DFo–mFc electron-density map contoured at 1σ level. (A) Face-to-face dimer [D1(A)]. (B) Back-to-back dimer [D2(A)]. (C) Extended dimer [D3(AB)].

one genetic study of *Bc*RsaM and two studies of related proteins have recently been published and provide suggestive evidence that RsaM may play a role in transcriptional regulation. In a study describing a homolog from the *B. cenocepacia* H111 strain, a transposon insertion between *bcam1869* and the adjacent *cepR* gene was compared with the parent strain using DNA microarrays [28]. This mutation altered the expression of 118 genes, although it was not clear whether the mutation affected *bcam1869*, or *cepR* or both. A null mutation in *bcam1869* was also constructed using an antibiotic resistance cassette, although this cassette could also influence expression of the flanking *cepR* and *cepI* genes. This mutant showed only mild decreases in swarming motility, biofilm formation, protease production and pathogenicity in *C. elegans*. Both mutations caused an increase in production of *N*-acyl-L-homoserine lactones. By contrast, *Bc*RsaM overexpression caused a decrease in AHL

production. Paradoxically, the transposon insertion caused a decrease in transcription of the AHL synthase gene *cepI*, suggesting that RsaM could act post-transcriptionally. Interestingly, expression of *Bc*RsaM in *E. coli* strongly blocked the activity of LuxR. This was not due to destruction of exogenous AHL signal molecules, suggesting an interaction between *Bc*RsaM and the LuxR protein or the *luxI* promoter.

The second study analyzed the RsaM protein from *P. fuscovaginae*, which is somewhat distantly related to *Bc*RsaM (32% identity). This plant-pathogenic bacterium encodes two LuxIR systems, one of which is composed of PfsR and PfsI [22]. The *pfsR* and *pfsI* pair flanks the *rsaM* gene. Random transposon mutants were screened for elevated production of AHL signals, yielding an insertion mutant in the *rsaM* gene. The defect was only partially complemented by a plasmid copy of *rsaM*, suggesting that the phenotype could be partly or fully due to *cis*-acting effects. When

the PfsIR system was reconstituted in *E. coli*, expression of RsaM decreased expression of a *pfsI–lacZ* fusion (although the data were not provided). The authors concluded that RsaM somehow inhibited the activity or expression of PfsR or PfsI. It is possible that *Bc*RsaM could have similar properties, despite their somewhat weak similarity.

Perhaps the most compelling genetic analysis was obtained using the *tofR*, *tofM* and *tofI* genes of the plant pathogen *B. glumae* [33]. TofM resembles *Bc*RsaM (60% identity). Single deletions of *tofR*, *tofM* or *tofI* reduced production of toxoflavin. A mutant lacking *tofR* and *tofI* showed a residual synthesis of toxoflavin, whereas a *tofR*, *tofI*, *tofM* triple-deletion mutant produced no detectable toxoflavin. An unmarked deletion of *tofM* in an otherwise wild-type chromosome also decreased toxoflavin production under some conditions, and this defect was fully complemented using a cloned copy of *tofM*. These data suggest a level of functional redundancy, in that TofR–AHL complexes can activate production of toxoflavin in the absence of TofM and that TofM can also do so in the absence of TofR–AHL complexes. The authors concluded that TofM is most likely a transcription regulator. The stimulation of transcription by TofM stands in contrast to the inhibitory effects described for *Bc*RsaM and RsaM. Therefore, it appears that the functional redundancy is obtained using different mechanisms. TofR regulates by binding to the TofI promoter and TofM regulates TofI by some other unknown mechanism.

Following the above evidence for transcription regulation, we analyzed *Bc*RsaM interaction with double-stranded DNA. The DNA promoter region in front of the *cepI* gene in *B. cenocepacia* carries a semi-palindromic sequence that could potentially serve as a regulator-binding site. However, EMSA experiments with *Bc*RsaM and four different DNA fragments containing the presumed *Bc*RsaM binding site showed no interaction even at 10-fold protein/DNA excess (data not shown). We also did not detect any nonspecific binding to double-stranded DNA. It remains possible that this protein could bind to one or more specific DNA sequences located elsewhere, but this is not consistent with a *cis*-acting element. The RsaM electrostatic surface potential is also inconsistent with DNA binding as no major positively charged patches are found needed for interaction with the phosphosugar backbone of the DNA duplex or RNA molecule.

In addition, *Bc*RsaM does not seem to interact with OHL – a cognate signaling ligand for the CepIR system that could influence the regulatory function of the protein. The presence of OHL did not influence RsaM

stability or the hydrodynamic properties, suggesting the lack of interaction (Fig. 3). By analogy to other transcription regulators, the ligand molecule might trigger the conformational or oligomerization state change of the protein, switching it from an active to nonactive state, or vice versa. Such a significant structural rearrangement should give a clear signal in differential scanning fluorimetry and also in dynamic light scattering assays. That is not the case for *Bc*RsaM, suggesting that its function is independent of OHL. Moreover, *Bc*RsaM does not contain DNA-binding structural motifs in the monomer (see above) and all reported possible combinations of dimers, so it is very likely that it does not interact with DNA directly. Similar transcription regulators have been described before, for example, mannose operon regulator MtlR [34] or TraM – another QS-related regulator [35]. We cannot exclude, however, that *Bc*RsaM influences the QS system at a posttranscriptional and/or post-translational level.

Conclusion

Previous genetic studies of the RsaM role in CepIR-based QS systems strongly suggested that the protein is a *cis*-acting transcription regulator. To further investigate this hypothesis, we examined *Bc*RsaM for interaction with the relevant ligand molecule, OHL, and the *cepI* promoter, however, no OHL and/or DNA binding was observed. Based on size-exclusion chromatography, dynamic light scattering and crystallographic data, *Bc*RsaM appears to form a dimeric assembly. The protein monomer reveals a novel fold, which lacks known DNA-binding motifs. Also none of the possible dimeric arrangements, including the most likely D2, bears recognizable DNA-interacting elements. Moreover, no other enzyme active site signatures or RNA-binding motifs have been detected [36] and the protein does not appear to contain cavities that could accommodate ligand molecules, like OHL. Hence, we propose that the action of RsaM might result from interactions with other components of the transcription or translation machinery rather than from direct association with the DNA promoter, which appears unlikely given the structural features and preliminary biochemical characterization.

Materials and methods

Cloning to vector *pMCSG73* and *in vitro* TVMV cleavage of NusA–BcRsaM fusion

The full length *bcam1869* gene from *B. cenocepacia* J2315 was amplified from the genomic DNA with KOD DNA

polymerase (Novagen, Madison, WI, USA) using conditions and reagents provided by the manufacturers and cloned into vector pMCSG73 according to the ligation-independent procedure [37,38]. Protein targets expressed from vector pMCSG73 are produced as C-terminal fusions to *E. coli* transcriptional factor NusA in the following form: NusA–(TVMV protease recognition site)–His$_6$–Strep tag-(TEV protease recognition site)–TARGET (NusA-ETVRFQ/S-HHHHHH-WSHPQFEK-ENLYFQ/SNA-TARGET) (the underlined sequence shows the TEV protease recognition site included in the PCR primer "/" indicates the actual cleavage site). The fusion is subsequently cleaved *in vitro* using TVMV protease by disrupting protein target expressing cells in the presence of TVMV protease-producing cells. The amount of TVMV, overexpressed in 1 L of growth media is sufficient to cleave the NusA–target fusion from 10 L of target producing bacteria. The cleavage process typically occurs within 2 h after the start of sonication.

Protein expression and purification

A bacterial culture of the *E. coli* BL21-Gold(DE3) strain carrying pMCSG73–*bcam1869* was grown in 1 L of enriched M9 medium [39] at 37 °C, shaking at 200 r.p.m. until it reached a D_{600} of 1.0. Inhibitory amino acids (25 mg each of L-valine, L-isoleucine, L-leucine, L-lysine, L-threonine, L-phenylalanine) and 70 or 90 mg of selenomethionine (SeMet) (Orion Enterprises, Wheeling, IL, USA) were added to the culture, which was then cooled to 4 °C for 60 min. Protein expression was induced by 0.5 mM isopropyl-β-D-thiogalactoside. The cells were incubated overnight at 18 °C, then harvested and resuspended in lysis buffer (500 mM NaCl, 5% glycerol, 50 mM Hepes pH 8.0, 20 mM imidazole, and 10 mM β-mercaptoethanol). To remove NusA, 3 mL of TVMV protease producing cells suspension ($D_{600} \sim 70$) was added to the target cells, which were then disrupted by sonication. Insoluble cellular material was removed by centrifugation. SeMet-labeled protein was purified using Ni-NTA affinity chromatography and the ÄKTAxpress system (GE Healthcare Biosciences, Pittsburg, PA, USA) as described previously [40,41]. This was followed by cleavage of the His$_6$ tag using recombinant His$_7$-tagged TEV protease and an additional step of subtractive Ni-NTA affinity chromatography to remove the protease, affinity tag, and any uncut protein. Native *Bc*RsaM was also produced using the same approach. The cells were grown in the presence or absence of 10 μM OHL using a mixture of M9 and LB media and both proteins were purified using the procedure described above. The pure proteins were concentrated using an Amicon Ultra-15 concentrator (Millipore, Billerica, MA, USA) in buffer A (20 mM Hepes pH 8.0, 250 mM NaCl, and 2 mM dithiothreitol). Protein concentrations were determined from the absorbance at 280 nm using a NanoDrop 1000 spectrophotometer (Thermo Scientific, Hanover Park, IL, USA).

Size exclusion chromatography

The molecular weight of *Bc*RsaM in solution was determined by size exclusion chromatography using a Dionex HPLC equipped with an AS temperature-controlled autosampler housing two 96-well plate sample racks, a GP50 Gradient Pump, a PDA-100 Photodiode Array Detector (Thermo Scientific, CA, USA), and a SRT SEC-150 column from Sepax Technologies (Newark, DE, USA). The column was equilibrated with buffer A and calibrated with aprotinin (6.5 kDa), ribonuclease A (13.7 kDa), carbonic anhydrase (29 kDa), ovalbumin (44 kDa), conalbumin (75 kDa), aldolase (158 kDa) and thyroglobulin (669 kDa). Thirty microliters of *Bc*RsaM at 5 mg·mL^{-1} in buffer A was loaded onto the column. The separation was carried out at room temperature at a flow rate of 1 mL·min^{-1} and absorbance at 280 nm was monitored. The calibration curve of K_{av} versus log molecular weight was prepared using the equation $K_{av} = (V_e - V_o)/(V_t - V_o)$, where V_e = elution volume for the protein, V_o = column void volume and V_t = total bed volume.

Differential scanning fluorimetry

A differential scanning fluorimetry assay was performed using a Bio-Rad CFX96 real-time thermal cycler (Hercules, CA, USA) to determine the thermal stability of *Bc* RsaM alone and with OHL. The following samples were prepared in 40 μL reactions containing 5× SYPRO Orange (Invitrogen S-6650, Invitrogen, Carlsbad, CA, USA): (1) 20 μM *Bc* RsaM control, (2) 20 μM *Bc* RsaM control containing 0.05% ethyl acetate and (3) 20 μM *Bc* RsaM with 50 μM OHL (prepared in ethyl acetate). Each sample was performed in triplicate. Samples were held at 25 °C for 1 min, then increased by 0.5 °C at 30 s intervals. A first derivative plot (–d(RFU)/dT) was used to determine the melt peaks.

Dynamic light scattering

Dynamic light scattering was used to determine the molecular mass distribution of *Bc*RsaM at 23 °C. RsaM was prepared in degassed crystallization buffer at 5 mg·mL^{-1}. Twenty microliters of RsaM was loaded onto a 384-well clear-bottom plate (Corning 3540, Corning, NY, USA). The plate was centrifuged at 172 × g for 2 min before loading into a DynaPro Plate Reader instrument (Wyatt Technology Corp., Goleta, CA, USA).

Dynamic light scattering was also used to determine the thermal stability of RsaM in the absence and presence of OHL. The following samples were prepared in 20 μL reactions: (1) RsaM (native) control and (2) RsaM with 50 μM OHL. The samples, at 5 mg·mL^{-1}, were centrifuged at 16 060 × g for 5 min. Each sample was loaded onto a 384-well clear-bottom plate and overlaid with 7 μL mineral oil. The plate was centrifuged at 172 × g for 2 min before

loading into a plate reader. Measurements were taken at 1 °C intervals between 25 and 55 °C. Melting curves were determined.

EMSA

EMSA was used to measure protein–nucleic acid interactions [42]. The assays were conducted using four oligonucleotides: a 145 bp fragment containing the *cepI* promoter containing an imperfect palindrome (underlined) (1) 5′-GG TTTTCAATCCCGTTGATCAAGAAACCGTTACCACG TCCCGAATGGCGTCTTTACGCCGTCAC<u>CCTGTAAG AGTTACCAGTTACAGG</u>CTCCTCGTGCCGCGCGCT GTAATGCACGCATACAAAAGCACAGATCCGAGGA CATCC—3′. This fragment was generated by PCR using two primers (5′-GGATGTCCTCGGATCTGTGCTTTT-3′ and 5′-GGTTTTCAATCCCGTTGATCAAGAAACC-3′). Three synthetic DNA hairpins containing possible binding sites for *Bc*RsaM were also used ((2) 5′-ATG<u>GCGTCTTT ACGCC</u>GTCCCCCACG<u>GCGTAAAGACGCC</u>AT-3′, (3) 5′-AC<u>CCTGTAAGAGTTACCAGTTACAGG</u>CTCCCCC AGC<u>CTGTAACTGGTAACTCTTACAGGG</u>T-3′ and (4) 5′-GTTACAGGCTCCTCGTGCCGCGCGCTGTAATCC CCCAT<u>TACAGCGCGCGGCACGAGGAGCCTGTAA</u> C-3′. Prior to the assay, DNA hairpins were heated to 90 °C for 1 min and then allowed to cool to 24 °C. Two *Bc*RsaM protein samples were used in EMSA, one produced in the absence of OHL and one produced in the presence of OHL. The samples were prepared in 10 μL reactions in which the DNA amount was constant at 40 ng per reaction. The protein/DNA ratio varied from 1 : 1, 1 : 5 and 1 : 10 and samples were size-fractionated by gel electrophoresis using 6% TBE DNA retardation native gels (Invitrogen EC63655BOX). The reaction for oligo (1) contained 2 μL of 5× binding buffer (Invitrogen E33075): 750 mM KCl, 0.5 mM dithiothreitol, 0.5 mM EDTA and 50 mM Tris pH 7.4. The reactions for oligos (2) to (4) contained 1 μL of 10× binding buffer: 100 mM Tris, 10 mM EDTA, 1 M KCl, 1 mM dithiothreitol and 50% glycerol. The samples were incubated at 37 °C for 30 min, then cooled on ice. Prior to loading samples onto the gels, 2 μL of EMSA gel-loading solution (Invitrogen E33075) was added to each sample, then centrifuged. The entire 12 μL volume of each sample was loaded onto the gels. The gels were stained for DNA using SYBR Green (Invitrogen E33075) for 20 min in the dark, then washed twice with 150 mL H_2O for 10 s before visualizing. The gels were then stained for protein using SYPRO Ruby (Invitrogen E33075) for 3 h in the dark, then destained with a solution containing 10% methanol and 7% acetic acid for 1 h before visualizing. Protein and DNA alone controls were run as well. As a positive DNA-binding control two DNA-binding proteins, LuxT [43] and OccR [44] were used with their known respective DNA-binding sites.

Crystallization

Both native and SeMet-labeled *Bc*RsaM were screened for crystallization conditions using a Mosquito liquid dispenser (TTP LabTech, Melbourne, UK) and sitting drop vapor diffusion technique in 96-well CrystalQuick plates (Greiner Bio-one, Monroe, NC, USA). The protein was set up at 16 °C using the MCSG 1–4 screens from Microlytic Inc. (Burlington, MA, USA). For each condition, 0.4 μL of protein and 0.4 μL of crystallization formulation were mixed and then equilibrated against 140 μL of the reservoir solution. The protein concentration varied depending on the preparation: native protein was set up at 54 mg·mL^{-1}, SeMet derivatives were set up at 47 and 52 mg·mL^{-1} for the protein expressed in the presence of 90 and 70 mg·mL^{-1} SeMet in the culture, respectively. The crystals appeared under a number of conditions. For structure solution and refinement, four crystal variants were ultimately used. Two of them were obtained for the protein grown in the presence of SeMet in the culture, designated as crystals X1 (90 mg·L^{-1} SeMet, 0.2 M calcium acetate, 0.1 M imidazole : HCl pH 8.0, 20% PEG1000) and crystals X4 (70 mg·L^{-1} SeMet, 0.2 M calcium acetate, 0.1 M Hepes : NaOH pH 7.5, 10% PEG8000). The other two crystals were for the native protein: crystals X2 (0.14 M lithium citrate, 19% PEG3350) and crystals X3 (0.27 M lithium citrate, 25% PEG3350).

Data collection

Crystals X1 were briefly soaked in a cryoprotectant solution containing 15% ethylene glycol in mother liquor. Crystals X2 were soaked in a solution containing 0.25 M lithium citrate, 30% PEG3350 and 0.7 M KI for 40 s. Crystals X3 were soaked in 1 mM K_2PtCl_4 (in 0.25 M lithium citrate, 30% PEG3350) for 10 min and for another 10 min in 10 mM K_2PtCl_4. After soaking, all of the derivatized crystals were cryoprotected in a 5% glycerol solution (in 0.25 M lithium citrate, 30% PEG3350) and flash-cooled in liquid nitrogen. Crystals X4 were cryoprotected in reservoir buffer supplemented with 10% glycerol. All X-ray diffraction experiments were performed at the Structural Biology Center 19-ID beamline at the Advanced Photon Source, Argonne National Laboratory. Datasets were collected at 100 K. Diffraction images were processed with the HKL3000 program suite [45]. The resulting *sca* files for crystals X1, X2 and X3 were directly fed into the AUTOSHARP program [46]. Structure factor intensities for crystals X4 were converted to amplitudes in CTRUNCATE [47] from the CCP4 package [48]. Crystals X1, X2 and X3 belong to crystal form 1 (*P*6$_2$22) while crystals X4 represent crystal form 2 (*P*6$_1$22), with a unit cell roughly twice as large as in form X1 due to parameter *c* doubling. Consequently, while form 1 contains one protein molecule in the asymmetric unit, form 2 accommodates two chains.

Structure solution

The structure was solved by the Multiple Isomorphous Replacement with Anomalous Scattering (MIRAS) approach as implemented in AUTOSHARP [46] followed by Molecular Replacement (MR) using PHASER [49]. Specifically, in the AUTOSHARP protocol, crystals X1 were treated as native, whereas crystals X2 and X3 as heavy atom derivatives. The procedure included initial data manipulation (converting intensities to amplitudes in TRUNCATE [47]), scaling (SCALEIT [50]), identification of the heavy atom sites (SHELXD [51]), phasing (SHARP [52]) density modification (SOLMON [53]) and automatic model building (ARP/WARP [54]). Five iodide and two platinum (II) sites were located and the results of phase determination are provided in Table 1. The automatic model building traced only 58 residues out of 147 and no side chains were assigned. This largely incomplete initial structure was fed into BUCCANEER [55] giving a model with 112 residues, in which side chains for 81 residues were autotraced. Despite significant

improvement, the model failed to refine against the crystal X1 reflection file and several regions of the electron density map were ambiguous, preventing further manual model building. The unsuccessful refinement could not be attributed to an incorrectly assigned space group and/or twinning, but the diffraction image did show unusual features manifesting in diffuse scattering, which suggests the possibility of order-disorder effects.

Therefore, the partial MIRAS model was used as a template for molecular replacement phasing of crystal form X4. MR solution was used to complete and refine the structure. Manual model rebuilding against electron density maps was performed in COOT [56], and crystallographic refinement was carried out in BUSTER [57]. The protocol included optimization of TLS parameters with seven groups per protein molecule. In the final structure, for chain A residues Thr2–Asp138 have been modeled, whereas chain B contains residues Ser3–Ile100 and Ala105–Asp138. The remaining residues are not well-defined in the electron density maps and have not been built. In addition to the pro-

Table 1. Data collection and refinement statistics.

Data collection				
Crystal	X1 (Native 1)	X2 (KI)	X3 (K$_2$PtCl$_4$)	X4 (Native 2)
Space group	$P6_2$22	$P6_2$22	$P6_2$22	$P6_1$22
Cell dimensions (Å)	$a = 66.6$ $c = 103.4$	$a = 66.4$ $c = 102.6$	$a = 66.7$ $c = 104.6$	$a = 69.1$ $c = 216.8$
Temperature (K)	100	100	100	100
Radiation source	APS, 19-ID	APS, 19-ID	APS, 19-ID	APS, 19-ID
Wavelength (Å)	0.9791	1.5498	1.0719	0.9793
Resolution (Å)[a]	30.00–2.00	50.00–1.87	50.00–2.75	50.00–2.30
	(2.03–2.00)	(1.90–1.87)	(2.80–2.75)	(2.35–2.30)
Unique reflections	9654 (466)	10 358 (143)	3970 (194)	14 517 (925)
R_{merge}[b]	0.049 (0.812)	0.044 (above 1)	0.043 (above 1)	0.059 (0.847)
$<I>/<\sigma I>$	42.4 (3.5)	49.8 (0.23)	61.3 (0.85)	42.0 (3.8)
Completeness (%)	92.2 (100)	88.5 (25.2)	99.8 (100)	99.8 (100)
Redundancy	10.7 (11.0)	11.4 (2.5)	19.1 (16.3)	13.5 (14.2)
Phasing (for resolution range 33.31–1.99 Å)				
Phasing power (acentric/centric)		1.33/1.14	0.65/0.69	
Phasing power (anomalous)		1.483	1.143	
FOM (acentric/centric)	0.36/0.38			
Refinement				
Resolution (Å)				20.20–2.30
Reflections work/test set				13688/725
R_{work}/R_{free}[c]				0.215/0.257
No of atoms protein/water				1967/31
Average B factor (Å^2) protein/water				65.3/51.5
r.m.s.d. from ideal				
Bond lengths (Å)				0.011
Bond angles (°)				1.07
Ramachandran statistics of φ/ψ angles (%)				
Most favored				98.5
Outliers				0
Molprobity score				1.18
Clashscore				0.77

[a] Values in parentheses correspond to the highest resolution shell. [b] $R_{merge} = \Sigma h \Sigma j |Ihj - <Ih>|/\Sigma h \Sigma j Ihj$, where Ihj is the intensity of observation j of reflection h. [c] $R = \Sigma h |Fo| - |Fc|/\Sigma h |Fo|$ for all reflections, where Fo and Fc are observed and calculated structure factors, respectively. Rfree is calculated analogously for the test reflections, randomly selected and excluded from the refinement.

tein molecules, 31 water molecules have been identified. The quality of the final protein model was verified by the MOLPROBITY server [58]. The refinement results are summarized in Table 1. The *Bc*RsaM atomic coordinates were deposited to the PDB under entry 4O2H.

Acknowledgements

Author contributions

KM performed crystallographic work and structural analysis; GC did expression, purification, crystallization and assays; SC and RJ did cloning; GB and AJ designed EMSA; KM, SW and AJ wrote the paper.

References

1 Vial L, Chapalain A, Groleau MC & Deziel E (2011) The various lifestyles of the *Burkholderia cepacia* complex species: a tribute to adaptation. *Environ Microbiol* **13**, 1–12.

2 O'Sullivan LA & Mahenthiralingam E (2005) Biotechnological potential within the genus *Burkholderia*. *Lett Appl Microbiol* **41**, 8–11.

3 Lipuma JJ (2005) Update on the *Burkholderia cepacia* complex. *Curr Opin Pulm Med* **11**, 528–533.

4 Vanlaere E, Baldwin A, Gevers D, Henry D, De Brandt E, LiPuma JJ, Mahenthiralingam E, Speert DP, Dowson C & Vandamme P (2009) Taxon K, a complex within the *Burkholderia cepacia* complex, comprises at least two novel species, *Burkholderia contaminans* sp. nov. and *Burkholderia lata* sp. nov. *Int J Syst Evol Microbiol* **59**, 102–111.

5 Vanlaere E, Lipuma JJ, Baldwin A, Henry D, De Brandt E, Mahenthiralingam E, Speert D, Dowson C & Vandamme P (2008) *Burkholderia latens* sp. nov., *Burkholderia diffusa* sp. nov., *Burkholderia arboris* sp. nov., *Burkholderia seminalis* sp. nov. and *Burkholderia metallica* sp. nov., novel species within the *Burkholderia cepacia* complex. *Int J Syst Evol Microbiol* **58**, 1580–1590.

6 Peeters C, Zlosnik JE, Spilker T, Hird TJ, LiPuma JJ & Vandamme P (2013) *Burkholderia pseudomultivorans* sp. nov., a novel *Burkholderia cepacia* complex species

from human respiratory samples and the rhizosphere. *Syst Appl Microbiol* **36**, 483–489.

7 Reik R, Spilker T & Lipuma JJ (2005) Distribution of *Burkholderia cepacia* complex species among isolates recovered from persons with or without cystic fibrosis. *J Clin Microbiol* **43**, 2926–2928.

8 Isles A, Maclusky I, Corey M, Gold R, Prober C, Fleming P & Levison H (1984) *Pseudomonas cepacia* infection in cystic fibrosis: an emerging problem. *J Pediatr* **104**, 206–210.

9 McClean S & Callaghan M (2009) *Burkholderia cepacia* complex: epithelial cell–pathogen confrontations and potential for therapeutic intervention. *J Med Microbiol* **58**, 1–12.

10 Subramoni S & Sokol PA (2012) Quorum sensing systems influence *Burkholderia cenocepacia* virulence. *Future Microbiol* **7**, 1373–1387.

11 Minagawa S, Inami H, Kato T, Sawada S, Yasuki T, Miyairi S, Horikawa M, Okuda J & Gotoh N (2012) RND type efflux pump system MexAB–OprM of *Pseudomonas aeruginosa* selects bacterial languages, 3-oxo-acyl-homoserine lactones, for cell-to-cell communication. *BMC Microbiol* doi:10.1186/1471-2180-12-70.

12 Kaplan HB & Greenberg EP (1985) Diffusion of autoinducer is involved in regulation of the Vibrio-Fischeri luminescence system. *J Bacteriol* **163**, 1210–1214.

13 Kohler T, van Delden C, Curty LK, Hamzehpour MM & Pechere JC (2001) Overexpression of the MexEF–OprN multidrug efflux system affects cell-to-cell signaling in *Pseudomonas aeruginosa*. *J Bacteriol* **183**, 5213–5222.

14 Tsai CS & Winans SC (2010) LuxR-type quorum-sensing regulators that are detached from common scents. *Mol Microbiol* **77**, 1072–1082.

15 Lutter E, Lewenza S, Dennis JJ, Visser MB & Sokol PA (2001) Distribution of quorum-sensing genes in the *Burkholderia cepacia* complex. *Infect Immun* **69**, 4661–4666.

16 Lewenza S, Conway B, Greenberg EP & Sokol PA (1999) Quorum sensing in *Burkholderia cepacia*: identification of the LuxRI homologs CepRI. *J Bacteriol* **181**, 748–756.

17 Gotschlich A, Huber B, Geisenberger O, Togl A, Steidle A, Riedel K, Hill P, Tummler B, Vandamme P, Middleton B *et al.* (2001) Synthesis of multiple *N*-acylhomoserine lactones is wide-spread among the members of the *Burkholderia cepacia* complex. *Syst Appl Microbiol* **24**, 1–14.

18 Malott RJ, Baldwin A, Mahenthiralingam E & Sokol PA (2005) Characterization of the cciIR quorum-sensing system in *Burkholderia cenocepacia*. *Infect Immun* **73**, 4982–4992.

19 Malott RJ, O'Grady EP, Toller J, Inhulsen S, Eberl L & Sokol PA (2009) A *Burkholderia cenocepacia* orphan

LuxR homolog is involved in quorum-sensing regulation. *J Bacteriol* **191**, 2447–2460.

20 Ryan GT, Wei Y & Winans SC (2013) A LuxR-type repressor of *Burkholderia cenocepacia* inhibits transcription via antiactivation and is inactivated by its cognate acylhomoserine lactone. *Mol Microbiol* **87**, 94–111.

21 Gelencser Z, Choudhary KS, Coutinho BG, Hudaiberdiev S, Galbats B, Venturi V & Pongor S (2012) Classifying the topology of AHL-driven quorum sensing circuits in proteobacterial genomes. *Sensors (Basel)* **12**, 5432–5444.

22 Mattiuzzo M, Bertani I, Ferluga S, Cabrio L, Bigirimana J, Guarnaccia C, Pongor S, Maraite H & Venturi V (2011) The plant pathogen *Pseudomonas fuscovaginae* contains two conserved quorum sensing systems involved in virulence and negatively regulated by RsaL and the novel regulator RsaM. *Environ Microbiol* **13**, 145–162.

23 O'Grady EP, Viteri DF & Sokol PA (2012) A unique regulator contributes to quorum sensing and virulence in *Burkholderia cenocepacia*. *PLoS One* **7**, e37611.

24 Weingart CL, White CE, Liu S, Chai Y, Cho H, Tsai CS, Wei Y, Delay NR, Gronquist MR, Eberhard A *et al.* (2005) Direct binding of the quorum sensing regulator CepR of *Burkholderia cenocepacia* to two target promoters *in vitro*. *Mol Microbiol* **57**, 452–467.

25 Wei Y, Ryan GT, Flores-Mireles AL, Costa ED, Schneider DJ & Winans SC (2011) Saturation mutagenesis of a CepR binding site as a means to identify new quorum-regulated promoters in *Burkholderia cenocepacia*. *Mol Microbiol* **79**, 616–632.

26 Choudhary KS, Hudaiberdiev S, Gelencser Z, Goncalves Coutinho B, Venturi V & Pongor S (2013) The organization of the quorum sensing luxI/R family genes in *Burkholderia*. *Int J Mol Sci* **14**, 13727–13747.

27 Venturi V, Rampioni G, Pongor S & Leoni L (2011) The virtue of temperance: built-in negative regulators of quorum sensing in *Pseudomonas*. *Mol Microbiol* **82**, 1060–1070.

28 Inhülsen S (2011) Investigations on the quorum sensing circuitry in *Burkholderia cenocepacia* H111. PhD dissertation, University of Zurich, Switzerland.

29 Holm L & Rosenstrom P (2010) Dali server: conservation mapping in 3D. *Nucleic Acids Res* **38** (Suppl), W545–549.

30 Jutras BL, Chenail AM, Rowland CL, Carroll D, Miller MC, Bykowski T & Stevenson B (2013) Eubacterial SpoVG homologs constitute a new family of site-specific DNA-binding proteins. *PLoS One* **8**, e66683.

31 Krissinel E & Henrick K (2007) Inference of macromolecular assemblies from crystalline state. *J Mol Biol* **372**, 774–797.

32 Kabsch W & Sander C (1983) Dictionary of protein secondary structure: pattern recognition of hydrogen-bonded and geometrical features. *Biopolymers* **22**, 2577–2637.

33 Chen R, Barphagha IK, Karki HS & Ham JH (2012) Dissection of quorum-sensing genes in *Burkholderia glumae* reveals non-canonical regulation and the new regulatory gene *tofM* for toxoflavin production. *PLoS One* **7**, e52150.

34 Tan K, Clancy S, Borovilos M, Zhou M, Horer S, Moy S, Volkart LL, Sassoon J, Baumann U & Joachimiak A (2009) The mannitol operon repressor MtlR belongs to a new class of transcription regulators in bacteria. *J Biol Chem* **284**, 36670–36679.

35 Chen G, Jeffrey PD, Fuqua C, Shi Y & Chen L (2007) Structural basis for antiactivation in bacterial quorum sensing. *Proc Natl Acad Sci USA* **104**, 16474–16479.

36 Laskowski RA, Watson JD & Thornton JM (2005) ProFunc: a server for predicting protein function from 3D structure. *Nucleic Acids Res* **33**, W89–W93.

37 Aslanidis C & de Jong PJ (1990) Ligation-independent cloning of PCR products (LIC-PCR). *Nucleic Acids Res* **18**, 6069–6074.

38 Eschenfeldt WH, Stols L, Millard CS, Joachimiak A & Mark ID (2009) A family of LIC vectors for high-throughput cloning and purification of proteins. *Methods Mol Biol* **498**, 105–115.

39 Stols L, Millard CS, Dementieva I & Donnelly MI (2004) Production of selenomethionine-labeled proteins in two-liter plastic bottles for structure determination. *J Struct Funct Genomics* **5**, 95–102.

40 Kim Y, Babnigg G, Jedrzejczak R, Eschenfeldt WH, Li H, Maltseva N, Hatzos-Skintges C, Gu M, Makowska-Grzyska M, Wu R *et al.* (2011) High-throughput protein purification and quality assessment for crystallization. *Methods* **55**, 12–28.

41 Kim Y, Dementieva I, Zhou M, Wu R, Lezondra L, Quartey P, Joachimiak G, Korolev O, Li H & Joachimiak A (2004) Automation of protein purification for structural genomics. *J Struct Funct Genomics* **5**, 111–118.

42 Kim Y, Ye Z, Joachimiak G, Videau P, Young J, Hurd K, Callahan SM, Gornicki P, Zhao J, Haselkorn R *et al.* (2013) Structures of complexes comprised of *Fischerella* transcription factor HetR with *Anabaena* DNA targets. *Proc Natl Acad Sci USA* **110**, E1716–1723.

43 Lin YH, Miyamoto C & Meighen EA (2000) Purification and characterization of a luxO promoter binding protein LuxT from *Vibrio harveyi*. *Protein Expr Purif* **20**, 87–94.

44 Wang L & Winans SC (1995) The sixty nucleotide OccR operator contains a subsite essential and sufficient for OccR binding and a second subsite

required for ligand-responsive DNA bending. *J Mol Biol* **253**, 691–702.

45 Minor W, Cymborowski M, Otwinowski Z & Chruszcz M (2006) HKL-3000: the integration of data reduction and structure solution – from diffraction images to an initial model in minutes. *Acta Crystallogr D Biol Crystallogr* **62**, 859–866.

46 Vonrhein C, Blanc E, Roversi P & Bricogne G (2007) Automated structure solution with autoSHARP. *Methods Mol Biol* **364**, 215–230.

47 French S & Wilson K (1978) Treatment of negative intensity observations. *Acta Crystallogr A* **34**, 517–525.

48 CCP4 (1994) The CCP4 suite: programs for protein crystallography. *Acta Crystallogr D Biol Crystallogr* **50**, 760–763.

49 McCoy AJ, Grosse-Kunstleve RW, Adams PD, Winn MD, Storoni LC & Read RJ (2007) Phaser crystallographic software. *J Appl Crystallogr* **40**, 658–674.

50 Howell PL & Smith GD (1992) Identification of heavy-atom derivatives by normal probability methods. *J Appl Crystallogr* **25**, 81–86.

51 Sheldrick GM (2008) A short history of SHELX. *Acta Crystallogr A* **64**, 112–122.

52 Bricogne G, Vonrhein C, Flensburg C, Schiltz M & Paciorek W (2003) Generation, representation and flow of phase information in structure determination: recent developments in and around SHARP 2.0. *Acta Crystallogr D Biol Crystallogr* **59**, 2023–2030.

53 Abrahams JP & Leslie AG (1996) Methods used in the structure determination of bovine mitochondrial F1 ATPase. *Acta Crystallogr D Biol Crystallogr* **52**, 30–42.

54 Langer G, Cohen SX, Lamzin VS & Perrakis A (2008) Automated macromolecular model building for X-ray crystallography using ARP/wARP version 7. *Nat Protoc* **3**, 1171–1179.

55 Cowtan K (2006) The Buccaneer software for automated model building. 1. Tracing protein chains. *Acta Crystallogr D Biol Crystallogr* **62**, 1002–1011.

56 Emsley P & Cowtan K (2004) Coot: model-building tools for molecular graphics. *Acta Crystallogr D Biol Crystallogr* **60**, 2126–2132.

57 Bricogne G, Blanc E, Brandl M, Flensburg C, Keller P, Paciorek W, Roversi P, Sharff A, Smart OS, Vonrhein C *et al.* (2011) BUSTER Version 2.10.0. Global Phasing Ltd., Cambridge.

58 Chen VB, Arendall WB III, Headd JJ, Keedy DA, Immormino RM, Kapral GJ, Murray LW, Richardson JS & Richardson DC (2010) MolProbity: all-atom structure validation for macromolecular crystallography. *Acta Crystallogr D Biol Crystallogr* **66**, 12–21.

59 Edgar RC (2004) MUSCLE: a multiple sequence alignment method with reduced time and space complexity. *BMC Bioinformatics* **5**, 113.

60 Gouet P, Robert X & Courcelle E (2003) ESPript/ENDscript: extracting and rendering sequence and 3D information from atomic structures of proteins. *Nucleic Acids Res* **31**, 3320–3323.

61 Pettersen EF, Goddard TD, Huang CC, Couch GS, Greenblatt DM, Meng EC & Ferrin TE (2004) UCSF Chimera – a visualization system for exploratory research and analysis. *J Comput Chem* **25**, 1605–1612.